Available online at www.sciencedirect.com
ScienceDirect
Journal of Crystal Growth 305 (2007) 201–210
JOURNAL OF CRYSTAL GROWTH
www.elsevier.com/locate/jcrysgro

Dynamical model of brushite precipitation

Cristina Oliveira[a], Petia Georgieva[b,*], Fernando Rocha[a], António Ferreira[a], Sebastião Feyo de Azevedo[a]

[a]*Department of Chemical Engineering, Faculty of Engineering, University of Porto, R. Dr. Roberto Frias, 4200-465 Porto, Portugal*
[b]*DETI/IEETA, University of Aveiro, Campus Universitario de Santiago 3810-193 Aveiro, Portugal*

Received 26 June 2006; received in revised form 27 March 2007; accepted 9 April 2007
Communicated by M. Uwaha
Available online 13 April 2007

Abstract

The objectives of this work are twofold. From academic point of view the aim is to build a dynamical macro model to fit the material balance and explain the main kinetic mechanisms that govern the transformation of the hydroxyapatite (HAP) into brushite and the growth of brushite, based on laboratory experiments and collected database. From practical point of view, the aim is to design a reliable process simulator that can be easily imbedded in industrial software for model driven monitoring, optimization and control purposes.

Based upon a databank of laboratory measurements of the calcium concentration in solution (on-line) and the particle size distribution (off-line) a reliable dynamical model of the dual nature of brushite particle formation for a range of initial concentrations of the reagents was derived as a system of ordinary differential equations of time. The performance of the model is tested with respect to the predicted evolution of mass of calcium in solution and the average (in mass) particle size along time. Results obtained demonstrate a good agreement between the model time trajectories and the available experimental data for a number of different initial concentrations of reagents.

Keywords: A1. Computer simulation; A1. Dynamical model; A1. Growth models; A1. Optimization; A1. Precipitation; A2. Growth from solutions

1. Introduction

The precipitation of calcium phosphate was studied by many authors under different conditions [1–3]. Depending on the temperature, the level of supersaturation, pH and initial concentration of reagents, one can obtain different calcium phosphate phases. One of them is the dicalcium phosphate dihydrate (DCPD) known also as brushite. DCPD is recognized as an important product in the application of fertilizers to soil and is studied mainly for its role in the physiological formation of calcium phosphates.

For the present investigation, the precipitation of DCPD was performed in a batch laboratory crystallizer. The precipitation was carried out by mixing equi-molar quantities of calcium hydroxide suspension and orthophosphoric acid solution. Five successive stages were repeatedly identified during a number of experiments performed with different initial reagent concentrations and each of them lasting for about 3 h [3]: (i) spontaneous precipitation of hydroxyapatite (HAP); (ii) complete dissolution of calcium and HAP growth; (iii) appearance of first nuclei of brushite; (iv) coexistence of HAP and brushite and (v) transformation of HAP into brushite and growth of brushite.

A simulation model representing the above stages of the process is of particular interest for the chemical industry and for understanding the calcium phosphate formation mechanisms. However, getting a unified dynamical model describing all identified process stages is still an open problem. The practical approach adopted in this research was to look for reliable mathematical approximations of the individual stages. Among them, modelling of the last stage is the most challenging issue because it has to represent simultaneously two kinetics phenomena. Brushite

*Corresponding author. Tel.: +351 93 670 6280; fax: +351 22 508 1632.
E-mail addresses: cprog@fe.up.pt (C. Oliveira), petia@det.ua.pt (P. Georgieva).

0022-0248/$ - see front matter © 2007 Elsevier B.V. All rights reserved.
doi:10.1016/j.jcrysgro.2007.04.016

Nomenclature

AM average (in mass) particle size (m)
C concentration of calcium in solution (mol/m^3)
C^* solubility (mol/m^3)
G linear growth rate (m/s)
J_{crys} precipitation rate (kg/s)
K_{HAP}, K_g optimization parameters
k_a area shape factor (dimensionless)
k_L proportional parameter (dimensionless)
k_{vHAP}, k_{vB} volume shape factor of brushite, HAP (dimensionless)
L_{HAP}, L_B crystal size of brushite, HAP (m)
mm_B, mm_C, mm_{HAP} molar weight of brushite, calcium in solution, HAP (kg/mol)
M_c calcium in solution (kg)
M_B, M_{HAP} mass of brushite, HAP in precipitate (kg)
$n(L)$ number–size distribution density function
P weighting factor (dimensionless)
q_{m1}, q_{m2} molar weight ratio, (calcium/HAP, brushite/HAP) (dimensionless)
R_g specific growth rate (kg/m^{2}s)
μ_j moments of number–size distribution
ρ_B, ρ_{HAP} density of brushite, HAP (kg/ m^3)
V volume (m^3)

grows due to direct consumption of calcium in the solution and due to the transformation of HAP into brushite. The transformation of HAP into brushite would not be expected since HAP is thermodynamically the most stable species. Nevertheless, at this stage HAP appears to be in a low-crystallinity state and in metastable equilibrium with brushite which provokes the transformation.

In this paper, a dynamical analytical model with respect to the last stage is proposed. To the best of our knowledge, there are no previous publications considering the issue of modelling the dual nature of brushite particle formation. In many previous works on growth kinetics of DCPD crystals as for example in Marshall and Nancollas [4], Hohl et al. [5] and Heughebaert et al. [6] the same process is studied in seeded solutions. Such a scenario impedes spontaneous nucleation and growth, which is in contrast to the study considered in this paper.

The present work is based on several contributions in different fields. Modelling of the general crystallization kinetics has been established by Randolph and Larson [7]. Kinetic parameter estimation based on the moment analysis techniques has been studied by Tavare and Garside [8]. The mechanisms that govern the formation of brushite were thoroughly investigated in a previous work by the authors (see Ref. [3]). In that paper, the experimental proofs for the identification of five distinct stages that explain the complete transformation into brushite, were reported. Models that combine analytical and data-driven approach to approximate the batch crystallization phenomenon have been developed in Ref. [9] (see also the contribution by Simoglou et al. [10]).

The paper is organized as follows: in Section 2 the experimental procedure of brushite precipitation is briefly discussed. In Section 3 a mathematical model of the process is introduced and the main theoretical motivations are stated. Section 4 contains details on the optimization procedure for model fitting. Finally, in Section 5 the theoretical model is evaluated by simulations and the results for optimization and validation data are illustrated.

2. Experimental procedure

Experiments [3,11] were performed in a batch reactive crystallization cylindrical tank made of glass, with 100 mm in diameter and 250 mm in height, and a glass stirrer operated at 270 rpm. Temperature was regulated by a water jacket and a thermostat bath maintained at 25 °C. The reactive crystallization of brushite was carried out by mixing equal volumes, 0.5 dm^3, of calcium hydroxide (Riedel–de Haën, 96%, 31219) aqueous suspension and orthophosphoric acid (Pronalab, 85%) aqueous solution with the same molar concentration. Ultra-pure water was used. The experiment began by quickly adding the calcium hydroxide suspension to the orthophosphoric acid solution. The concentration of reagents, before mixing, varied from 0.05 to 0.4 M. The calcium concentration, pH, temperature and conductivity were continuously measured (inoLab pH/Cond Level 3, WTW) and recorded by a computer for about 3 h. Suspension samples were withdrawn at different time intervals, filtered, dried and analyzed by scanning electron microscope (SEM) and characterized by X-ray diffraction. The calcium was analyzed using a selective electrode (WTW-D82362 Weitheim), and pH was measured by an electrode WTW Sentix 6. X-ray diffraction was made with a Philips PW1830 diffractometer using the CoK_α radiation ($\lambda_{CoK_\alpha} = 0.1789$ nm). The particle size distribution is periodically determined by laser light diffraction (with a Coulter laser particle granulometer). As a result, a database with the evolution of the particle size distribution along time was recorded. Table 1 summarizes partially the data for the average (in mass) particle size (AM) and the time of probes for two initial concentrations (0.05 and 0.4 M).

3. Dynamical model

The evolution in time of the overall process of DCPD precipitation is governed by distinct driving forces. Therefore, attempts to represent all phases by a common model

Table 1
Partial data set of AM

Init. concentration		Init. concentration	
0.4 M		0.05 M	
Time (s)	AM (μm)	Time (s)	AM (μm)
180	22.39	600	15.37
300	22.41	1500	16.10
480	25.22	2100	16.37
600	26.54	2400	15.50
780	27.61	3000	15.98
900	26.86	3495	16.45
1080	26.71	3600	16.67
1200	26.37	4380	19.25
1380	26.88	4395	18.58
1680	27.35	4920	18.98
2100	25.55	5400	20.83
2400	25.65	5520	19.71
3000	26.32	6000	22.66
3300	25.45	6120	21.52
3600	25.52	6195	22.98
4500	27.06	7200	24.92
5400	26.63	7260	25.42
6300	26.43	7340	24.59
7411	25.44	7695	25.73
8280	25.63	8640	25.16
9018	25.61	9120	26.44
10 020	25.31	9600	27.29
10 821	25.70	10 800	28.08
11 280	25.89	11 040	26.40

do seem not relevant. In a previous work [3] all experimentally identified phases were thoroughly discussed and the process evolution (along 3 h) was divided into five stages:

(1) In the overall process of DCPD precipitation the first compound to be formed is HAP. In this first stage there is an equilibrium between HAP precipitated and HAP in solution. The HAP growth and pH stabilization are essentially due to the consumption of calcium not yet dissolved into the solution.
(2) The calcium is completely dissolved, and consequently the HAP growth is responsible for the pH decrease.
(3) As pH changes the first nuclei of brushite appear.
(4) Two species, brushite and HAP, coexist in the solution.
(5) Brushite becomes the most stable species in the solution and a transformation of HAP into brushite occurs. Brushite growth is stabilized.

In the last stage of the process, a slow increase in pH and a decrease in calcium concentration was observed. SEM and X-ray diffraction analyses showed a gradual reduction of HAP crystals simultaneously with the growth of brushite crystals, until the complete HAP disappearance. This happens because HAP is in a low crystallinity state and in metastable equilibrium with brushite. Since the brushite crystallization rate is much higher than the HAP crystallization rate, the kinetics factors have a crucial role leading to the gradual HAP disappearing and brushite formation. Consequently, the HAP-brushite transformation leads to pH increase. Fig. 1 [3] refers to three different moments of this stage. The HAP disappearance and the consequent increase in brushite crystallinity are clearly visible. The experiments confirmed that brushite particles grow due to the calcium consumption in the solution and due to a transformation of HAP into brushite. This dual kinetic nature of brushite precipitation constitutes the main modelling challenge.

Since the transformation from HAP into brushite is a chemical reaction, which has a lot of influence on the composition of the solution, the speciation of the solution was explicitly taken into account during the process study (see Appendix A). This was made by solving a system of equilibrium and mass balance equations and from the measurements of calcium concentration and pH [11]. The system describes the chemical species present in the solution, and the change of their concentrations along time. Based on this system, presented in more details in Appendix A, the composition of the precipitate was also determined and the mass conservation equation (2) of the model that follows was extracted.

The model is conceptually obtained by writing the appropriate mass balances with a mathematical representation of the precipitation rate. The latter can be achieved applying basic mass transfer considerations [12] or by writing a population balance represented by its moment equations [13,14].

At first glance the method of population balance seems not quite typical to describe HAP–brushite transformation mainly because it assumes the presence or the introduction of seeds to induce the particle growth. However, based on the available images showing brushite appearance on the surface of HAP crystals, the existing HAP particles at the beginning of the fifth phase can be interpreted as seeds for brushite formation. Furthermore, the method of population balance represented by its moments was preferred since it allows taking into account initial experimental distributions for which data are available.

Process modelling involves the following assumptions: (i) the suspension is well mixed in the whole tank volume; (ii) the suspension volume is constant during the precipitation process.

3.1. Mass balances

The following set of conservation mass balance Eqs. (1)–(4) includes mass of calcium in solution (M_c), mass of HAP particles (M_{HAP}), mass of brushite particles (M_B), with respective molar weight ratios (q_{m1}, q_{m2}):

$$\frac{dM_c}{dt} = -q_{m1} J_{crys}, \tag{1}$$

$$\frac{dM_{HAP}}{dt} = -K_{HAP}(M_{HAP})^2, \tag{2}$$

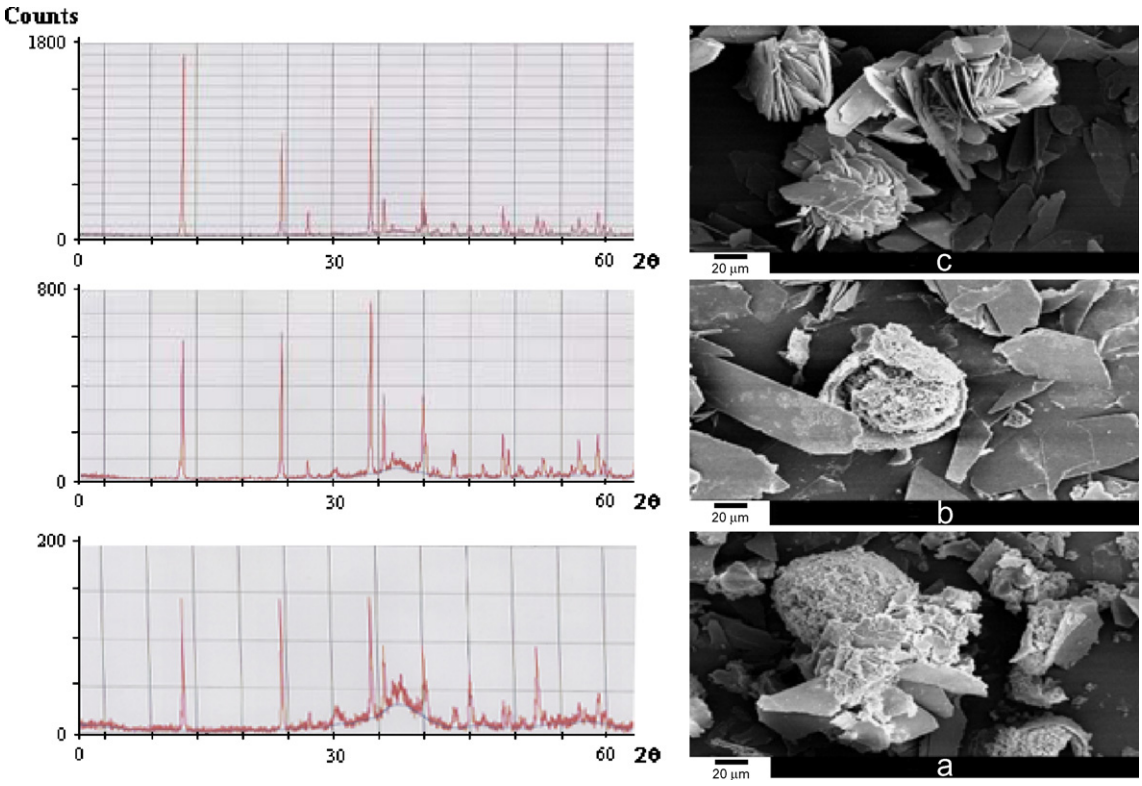

Fig. 1. Time evolution of crystallinity in the last stage: (a) initial, (b) middle, (c) final [3].

$$\frac{dM_B}{dt} = J_{crys} + 10q_{m2}K_{HAP}(M_{HAP})^2, \quad (3)$$

$$q_{m1} = \frac{mm_c}{mm_B}, \quad q_{m2} = \frac{mm_B}{mm_{HAP}}. \quad (4)$$

In Eq. (2), M_{HAP} is determined as a monotonically decreasing function, which corresponds to the experimentally observed HAP dynamical behavior. K_{HAP} is one of the model fitting parameters. The second order was chosen after an optimization procedure to get qualitative curve fitting of the available measurements for all initial concentrations.

Based on system (A.1) presented in Appendix A, the available measurements and the given initial concentrations of calcium and phosphates, the concentration of all chemical species in solution were determined and then used to calculate the mass and composition of precipitate along time, more particularly Eqs. (2) and (3).

HAP is the first precipitate to be formed and during the last stage all HAP particles gradually transform into brushite particles according to the following reaction equation:

$$Ca_{10}(OH)_2(PO_4)_6 + 4H_3PO_4 + 18H_2O \rightarrow 10CaHPO_4 \cdot 2H_2O.$$

The transformation of HAP into brushite was quantified by calculating the calcium to phosphate molar ratio ($R = Ca/P$) in the precipitate. Initially this ratio was equal to 1.67 (which means only HAP is present) and along time as HAP transforms into brushite the ratio decreases monotonically until it reaches the value of 1 (all HAP is transformed into brushite). The number of particles during this (last) stage of transformation was estimated by the particle size distribution periodic measurements and the calculated mass of precipitate. It was practically constant along the stage. This is the first phenomenon modelled by Eq. (3), mathematically expressed by the right-hand term $10q_{m2}K_{HAP}(M_{HAP})^2$.

Based on the measurements it was further observed that the solution is supersaturated relatively to brushite and the calcium concentration decreases along the time, which means brushite particles grow from solution. This is the second phenomenon modelled in Eq. (3) and expressed by the term J_{crys}.

In summary, Eq. (3) follows from the speciation relations given in Appendix A and more particularly from the concentrations of the different chemical species in solutions (measured as the calcium, or determined from the system of equations (A.1)).

In this way Eq. (3) reflects the dual nature of brushite mass balance. On one hand, brushite mass increases due to direct consumption of calcium in the solution (J_{crys} is proportional to $-dM_c/dt$) and on the other hand more brushite is formed due to HAP–brushite transformation ($K_{HAP}(M_{HAP})^2$ is proportional to HAP mass decrease$-dM_{HAP}/dt$).

3.2. Population balance

The difficulty in precipitation modelling is essentially due to the accurate description of the kinetics involved [15,16]. This particular kinetics model involves some simplifying assumptions experimentally confirmed by periodical laser light diffraction measurements: (i) during the last phase of DCPD precipitation the number of crystals does not change significantly; (ii) growth rate is independent of the crystal size; (iii) agglomeration and breakage phenomena are negligible and therefore were not considered for modelling. Before analysis by SEM and X-ray diffraction the suspension samples are filtered and dried. During the filtration process the particles tend to aggregate. Therefore, the SEM images in Fig. 1 show the particles as if they were agglomerated. In fact they are only aggregated and are afterwards easily dispersed in an ultra-sonic bath performed before the size measurements in the laser granulometer. The assumption (iii) is based on the laser measurements which confirm the lack of particle agglomeration.

For the evolution of the particle size distribution (PSD) the approach of Ref. [7] is adopted and the population balance is determined in terms of the number–size density function $n(L)$

$$\frac{\partial n(L)}{\partial t}+\frac{\partial(Gn(L))}{\partial L}=0. \tag{5}$$

Following the theory of Randolph and Larson [7], the partial differential equation (5) is conveniently replaced by the method of moments where each moment of the number–size distribution $n(L)$ is mathematically defined as

$$\mu_j(L)=\int_0^\infty L^j n(L)\mathrm{d}L, \quad j=0,1,2,3,\ldots. \tag{6}$$

The PSD evolution is recovered based on the first five moments determined by the following set of ordinary differential equations (ODE):

$$\frac{\mathrm{d}\mu_0}{\mathrm{d}t}=0, \tag{7}$$

$$\frac{\mathrm{d}\mu_1}{\mathrm{d}t}=G\mu_0, \tag{8}$$

$$\frac{\mathrm{d}\mu_2}{\mathrm{d}t}=2G\mu_1, \tag{9}$$

$$\frac{\mathrm{d}\mu_3}{\mathrm{d}t}=3G\mu_2, \tag{10}$$

$$\frac{\mathrm{d}\mu_4}{\mathrm{d}t}=4G\mu_3. \tag{11}$$

Eq. (7) reflects the assumption for lack of secondary nucleation. The zero moment (μ_0), which represents the number of crystals is assumed constant. This statement is experimentally grounded because PSD, periodically determined by laser light diffraction (Coulter Counter), confirmed that the number of the crystals did not change significantly.

The process nonlinearity is included in the precipitation rate J_{crys}, which is a function of the population balance as follows:

$$J_{\mathrm{crys}}=3\rho_{\mathrm{B}}k_{v\mathrm{B}}G\mu_2. \tag{12}$$

3.2.1. Brushite particle growth due to consumption of calcium in solution (path 1)

The kinetics of the brushite particle growth due to consumption of the calcium into solution is described by the linear growth rate (G)

$$G=\frac{k_{\mathrm{a}}R_{\mathrm{g}}}{3\rho_{\mathrm{B}}k_{v\mathrm{B}}}, \tag{13}$$

where R_{g} is the specific growth rate, defined as a second-order function of the relative supersaturation

$$R_{\mathrm{g}}=K_{\mathrm{g}}\left(\frac{C-C^*}{C^*}\right)^2 \tag{14}$$

K_{g} is one of the model fitting parameters.

Remark. In some publications (see Ref. [17]), for solutions of sparingly soluble salt such as HAP and DCPC, the crystallization driving force is expressed as a Gibbs free energy of transfer from supersaturated to saturated solution for a given solute. However, the supersaturation expression $C-C^*/C^*$ in Eq. (14) is also relevant as for example in Sohnel and Mullin [18] where the expression ([Ca]–[Ca]eq) is used as the driving force for the precipitation of calcium carbonate.

3.2.2. Brushite particle growth due to the HAP–brushite transformation (path 2)

Invoking general relations between the mass (m), the volume (V) and the linear size (L) of a particle

$$m=\rho V, \quad V=k_vL^3$$

the expression for L can be rearranged as

$$L=\left(\frac{m}{\rho k_v}\right)^{1/3}. \tag{15a}$$

Following (15a), the linear size of a HAP particle (L_{HAP}) and of a brushite particle (L_{B}) that correspond to a certain quantity of mass m is

$$L_{\mathrm{HAP}}=\left(\frac{m}{\rho_{\mathrm{HAP}}k_{v\mathrm{HAP}}}\right)^{1/3}, \quad L_{\mathrm{B}}=\left(\frac{m}{\rho_{\mathrm{B}}k_{v\mathrm{B}}}\right)^{1/3}, \quad L_{\mathrm{HAP}}\neq L_{\mathrm{B}}. \tag{15b}$$

From (15b), L_{B} can be determined as a function of L_{HAP} as follows:

$$L_{\mathrm{B}}=\left(\frac{\rho_{\mathrm{HAP}}k_{v\mathrm{HAP}}}{\rho_{\mathrm{B}}k_{v\mathrm{B}}}\right)^{1/3}L_{\mathrm{HAP}}=k_LL_{\mathrm{HAP}}, \tag{16}$$

where

$$k_L=\left(\frac{\rho_{\mathrm{HAP}}k_{v\mathrm{HAP}}}{\rho_{\mathrm{B}}k_{v\mathrm{B}}}\right)^{1/3}=1.4205. \tag{17}$$

The physical interpretation of Eqs. (16) and (17), from a mass balance point of view, is that the transformation of a certain quantity of HAP species into the same quantity of brushite species results into an enlargement of the linear particle size quantified by the parameter k_L. Obviously, the reason behind this is the different densities of the two species.

So far, the growth of brushite due to the two precipitation phenomena is analytically formulated implementing different mathematical approaches, path 1 is represented by the linear growth rate (13) and path 2 is accounted by the linear particle size (16). A possible way to explain simultaneously the two precipitation paths goes through the concept of the average (in mass) particle size (AM). Moreover, data for AM is available by the periodical laser light diffraction measurements. According to Randolph and Larson [7], AM can be determined as a function of the leading moments as follows:

$$\mathrm{AM} = \mu_4/\mu_3. \tag{18}$$

Expression (18) accounts for the brushite growth only due to consumption of calcium in the solution. Numerical simulations of the model with AM calculated by (18) show clearly a discrepancy between the experimental and simulated particle size distribution. The particle growth due to the HAP–brushite transformation as discussed in Eq. (16) needs also to be considered. To handle the problem we introduce in Eq. (18) a proportional factor (P) which is a function of k_L, in the form

$$\mathrm{AM} = P(k_L)\frac{\mu_4}{\mu_3}. \tag{19}$$

To find a suitable $P(k_L)$, an alternative form of computing the average (in mass) particle size is invoked (see Ref. [19])

$$\mathrm{AM} = \frac{\sum_{i=1}^{p} L_i M_i}{\sum_{i=1}^{p} M_i}, \tag{20}$$

where p is the number of different particle sizes in the assumed PSD, termed also as classes, M_i and L_i are the total mass and the respective particle size of class i. At each moment of the HAP–brushite transformation process, HAP and brushite particles coexist. Therefore, in order to obey the mass balance principle, the expression L_iM_i in Eq. (20) must be expressed as a sum of two terms corresponding to the respective portion of each species

$$L_i M_i = L_{\mathrm{B}i} M_{\mathrm{B}i} + L_{\mathrm{HAP}i} M_{\mathrm{HAP}i}. \tag{21}$$

Assuming Eq. (16) for each class it follows:

$$L_{\mathrm{B}i} = k_L L_{\mathrm{HAP}i}. \tag{22}$$

Taking into account Eqs. (21)–(22), Eq. (20) is modified as

$$\mathrm{AM} = \frac{\sum_{i=1}^{p} L_{\mathrm{HAP}i}(k_L M_{\mathrm{B}i} + M_{\mathrm{HAP}i})}{\sum_{i=1}^{p}(M_{\mathrm{B}i} + M_{\mathrm{HAP}i})}. \tag{23}$$

To get an expression for AM that describes the dual nature of brushite particle growth and considering Eqs. (19) and (23), the following proportional factor was selected:

$$P(k_L) = \frac{k_L M_{\mathrm{B}} + M_{\mathrm{HAP}}}{M_{\mathrm{B}} + M_{\mathrm{HAP}}}. \tag{24}$$

Expression (24) was obtained as a first-order approximation of the integral of Eq. (23).

4. Parameter fitting

The parameters, K_{HAP} and K_{g}, are fitted with data set obtained by a number of experiments with two different initial concentrations of reagents (0.2 and 0.3 M), following a classical non-linear regression. Each iteration of the optimization procedure includes the integration along time of balance Eqs. (1)–(3) and (7)–(11) for each of the experiments, with the required resetting of initial conditions for each run. The optimization is carried out in a batch mode, where the tuning parameters are updated only after complete processing of the whole data set and related computing of the performance function.

4.1. Performance function

The collected measurements of calcium concentration (on-line) and AM (off-line analysis) along time are the principal indicators for evaluation of the model quality. Therefore, both of them are integrated into the performance function. For each discrete time point k, the mass of calcium in the solution $(M_{\mathrm{c}}^{\mathrm{mod}})_k$ computed by Eq. (1) is compared with the available data $(M_{\mathrm{c}}^{\mathrm{data}})_k$ to determine the first error term of the performance function. For numerical reasons, its normalized form is preferred as follows:

$$E_k^{\mathrm{Ca}} = \frac{|(M_{\mathrm{c}}^{\mathrm{data}})_k - (M_{\mathrm{c}}^{\mathrm{mod}})_k|}{(M_{\mathrm{c}}^{\mathrm{data}})_k}. \tag{25}$$

The error between the model predictions (23) of $(\mathrm{AM}_k^{\mathrm{mod}})$ and the data $(\mathrm{AM}_k^{\mathrm{data}})$ for the average (in mass) particle size forms the second term of the performance function The respective normalized form is

$$E_k^{\mathrm{AM}} = \frac{\left|\mathrm{AM}_k^{\mathrm{data}} - \mathrm{AM}_k^{\mathrm{mod}}\right|}{\mathrm{AM}_k^{\mathrm{data}}}. \tag{26}$$

Note that the available data points for the trajectory of AM along time are much less than the values computed by the model. 40–60 AM data points correspond to the number of repetitions of the same experiment while 1600 (in average) AM model points correspond to the discretization time. In order to complete the data set with extra points required by Eq. (26), a theoretical curve was generated applying cubic spline interpolation on the initial data set. Finally, the performance function to be minimized has the following structure:

$$J = \sum_{j=1}^{N_{\mathrm{exp}}} \sum_{k=1}^{N_{\mathrm{points}}} [r_1(E_k^{\mathrm{Ca}})_j + r_2(E_k^{\mathrm{AM}})_j], \tag{27}$$

where r_1 and r_2 are factors that determine the priority of each term. For the present study both terms are considered as equally important and $r_1 = r_2 = 0.5$. Data from 6 repeating experiments with initial concentration of reagents 0.2 M and the same number of experiments with initial concentration of reagents 0.3 M were utilized for minimization of Eq. (27), hence $N_{exp} = 12$ and $N_{points} \approx 1600$.

4.2. Optimization scenario

The optimization procedure can be mathematically formulated as

$$\min_{K_{HAP} \in X, K_g \in Y} J. \tag{28}$$

The objective is to find the parameters $K_{HAP} \in X$ and $K_g \in Y$ known also as the decision variables that locally minimize (27). X and Y are closed intervals in R, which define the parameter sub-plane over which the optimal values are searched. The optimization procedure was performed in *Matlab* programming environment, with implementation of *Optimization* toolbox routines. The fourth order Runge–Kutta routine with variable step size was used for integration of the model Eqs. (1)–(3) and (7)–(11) and the simplex direct search method for the parameter adaptation. Due to the inherent stiffness of the model equations, numerical problems might appear. To overcome them and also to improve the convergence of the procedure a good choice of the initial values for K_{HAP} and K_g was required. Therefore, prior to the main two-dimensional optimization stage (28), a one-dimensional preliminary optimization was repeatedly performed. One of the parameters was fixed and the other served as a scalar local minimizer of Eq. (27) and then vice versa. The effectiveness of this preliminary step cannot be analytically proved, however it was observed that starting the main optimization stage with initial values of K_{HAP} and K_g determined by the individual parameter optimization speeded up the convergence.

4.3. Initial conditions

The initial conditions for the numerical simulations are summarized in Table 2. Recorded data are with respect to the overall precipitation process. However, since the objective of this work is to develop a model only for the transformation of HAP into brushite and growth of brushite, the simulations start at the beginning of the fifth stage. In order to get the initial values required for the integration of Eqs. (1)–(3), the initial time t_{ini} of the last process stage need to be extracted. The time point where pH starts slowly to increase and the calcium concentration starts slowly to decrease is assigned as an indicator for the beginning of the last stage. Once t_{ini} is determined, the initial values of the process states, $M_c(t_{ini})$, $M_{HAP}(t_{ini})$ and $M_B(t_{ini})$, are easily extracted from the data set. For the integration of the population balance Eqs. (7)–(11), the initial conditions of the leading moments are also required. To recover them, the general definition of the j moment of the number–size distribution is involved

$$\mu_j(L) = \int_0^\infty L^j n(L) \mathrm{d}L. \tag{29}$$

The first-order approximation of Eq. (29) is

$$\mu_j(L) = \sum_{i=1}^{p} (L_i^{mean})^j n_i(L) \Delta L_i, \tag{30}$$

where $\Delta L_i = |L_{i+1} - L_i|$ and $L_i^{mean} = (L_{i+1} + L_i)/2$.

The particles are distributed into p different sizes and for the case considered $p = 16$. The periodical measurements by the Coulter laser particle granulometer provide data for $n_i(L)$and (L_i), thus the $\mu_j(t_{ini})$ are straightforward recovered applying Eq. (30).

The final values of the optimized parameters and the values of constant parameters are summarized in Table 3.

Table 2
Initial conditions

Init. concentration of reagents (M)	Initial simulation time (s)	AM (μm)	pH	M_c (kg)	T (°C)	M_{HAP} (kg)	M_B (kg)
0.05	5400	20.83	5.72	1.614×10^{-4}	25.1	0.0015	0.00098
0.1	2100	21.30	5.5	2.215×10^{-4}	25.3	0.0023	0.00036
0.2	540	20.26	5.04	5.366×10^{-4}	25.7	0.00819	0.00035
0.3	390	22.06	4.65	6.358×10^{-4}	26.9	0.01257	0.00056
0.4	300	22.39	4.55	6.362×10^{-4}	28.2	0.0135	0.00079

Table 3
Values of constant and optimized model parameters

mm_B (kg/mol)	mm_C (kg/mol)	mm_{HAP} (kg/mol)	ρ_B (kg/m^3)	ρ_{HAP} (kg/m^3)	k_a	k_{vHAP}	k_{vB}	K_g	K_{HAP}
0.172	0.04	1.004	2304	3156	4.75	0.5236	0.25	0.2×10^{-5}	0.323

5. Results and discussion

The analytical model introduced in Section 3 is evaluated for its ability to predict process behavior for various initial concentrations of reagents (0.05, 0.1, 0.2, 0.3, and 0.4 M). The results are summarized in Figs. 2 and 3. Data for the main system states (M_c, M_{HAP} and M_B) are denoted by dashed line in all figures on subplots (a), (c) and (d), respectively. Data for AM is denoted by stars in all subplots (b). The model time trajectories of M_c (subplots (a)) and AM (subplots (b)) are direct indicators of the model quality since measurements for them are available. The mass of HAP and brushite are not directly measured variables but they can be inferred by the available

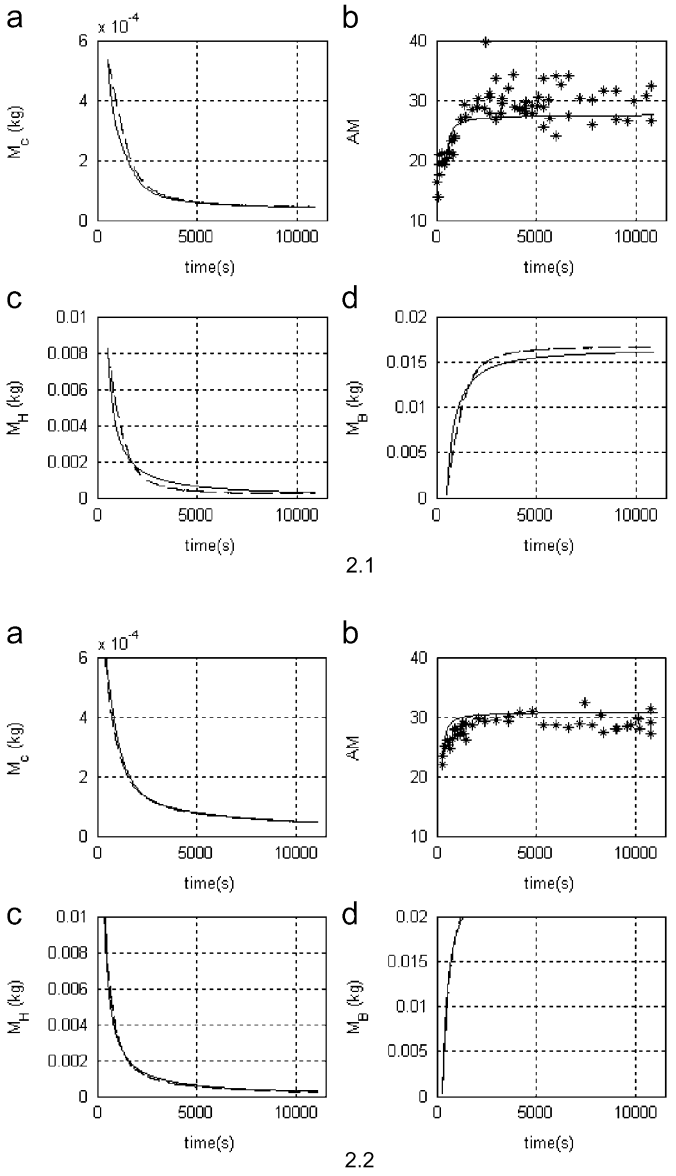

Fig. 2. (MODEL FITTING DATA) Data points (dashed line/stars) and model curves (solid line) along time for: (a) mass of calcium in solution, (b) the average size AM (μm); (c) mass of HAP; (d) mass of brushite (2.1) Initial concentration of reagents 0.2 M; (2.2) Initial concentration of reagents 0.3 M.

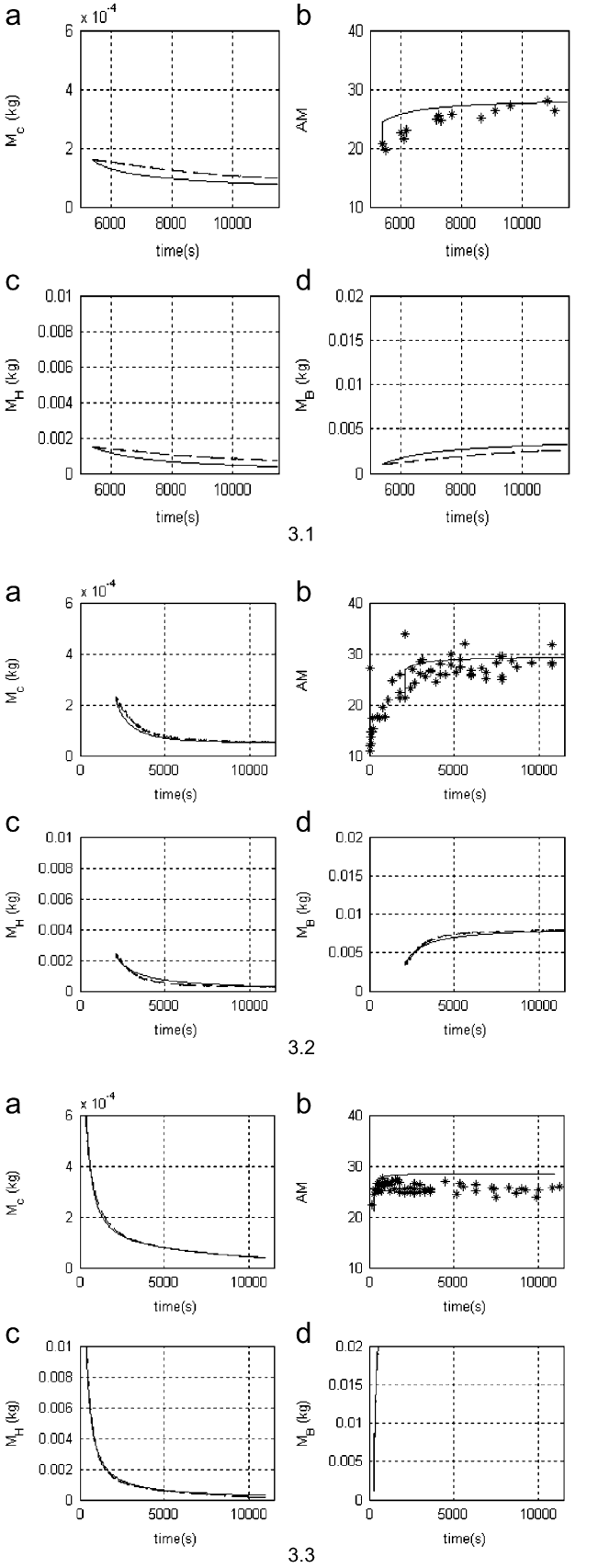

Fig. 3. (MODEL VALIDATION DATA) Data points (dashed line/stars) and model curves (solid line) along time for (a) mass of calcium in solution, (b) the average size AM (μm); (c) mass of HAP; (d) mass of brushite (3.1) Initial concentration of reagents 0.05 M; (3.2.) initial concentration of reagents 0.1 M; (3.3) initial concentration of reagents 0.5 M.

measurements. Thus, the plots of M_{HAP} (subplots (c)) and M_B (subplots (d)) are indirect indicators of the model reliability. Data from experiments with initial concentrations of reagents 0.2 and 0.3 M were used in Section 4 to optimize the model parameters, therefore it is not surprising that all model variables (M_c, M_{HAP}, M_B, AM) closely match the data from these two types of experiments (see Fig. 2). However, more valuable are the results depicted in Fig. 3 where the model was tested on new 'unseen' validation data corresponding to experiments with different initial concentrations (0.05, 0.1 and 0.4 M). Data and model trajectories match quite well which confirms the ability of the dynamical first principles model discussed in this work to simulate the physical phenomena of simultaneously HAP transformation into brushite and growth of brushite.

Remark. Variation of initial concentrations of the reagents results in changing the initial time of the last process stage (t_{ini}). Lower the concentration, later the beginning of HAP–brushite transformation.

6. Conclusions

A general dynamical model of the precipitation of dicalcium phosphate dehydrate is presented in this paper. The objective was to define a reliable model to explain the last stage of the overall precipitation process, namely the transformation of hydroxyapatite into DCPD (named as brushite) and the growth of brushite. Based upon a databank of laboratory measurements of the calcium concentration in the solution (on-line) and the particle size distribution (off-line) a dynamical model of the process for a range of initial concentrations of the reagents was derived as a system of ordinary differential equations of time. The performance of the model is examined with respect to prediction quality of the time trajectories of mass of calcium in the solution and the average (in mass) particle size.

Accurate prediction of brushite particles growth is directly related to reliable computation of the process states associated with mass and population balances, which was easily obtained. However, the main modelling challenge was to express the particle growth as a result of simultaneous consumption of calcium in the solution and transformation of HAP into brushite. The main contribution of this work is the kinetics model proposed which belongs to the general class of crystallization kinetics models for which well established theoretical background exists. At the same time the model preserves the physical transparency of the modelled phenomena.

We are aware that the dynamical model presented in this paper is only one possible approach to the mathematical interpretation of the dual phenomena of brushite precipitation. It could be somehow considered as imperfect because of insufficient fundamental knowledge in this area. However, our objectives were twofold. From academic point of view the aim was to build a macro model to fit the material balance and explain the main kinetic mechanisms that govern the transformation of the hydroxyapatite into brushite based on a long term laboratory experience and collected large database. From practical point of view, the aim of this modelling exercise was to design a reliable process simulator that can be easily imbedded in industrial software for model-based monitoring, optimization and control purposes. Therefore, the model developed is of particular importance not only for the academic understanding of calcium phosphate formation mechanisms but also for practical purposes of the chemical industry. Research on process monitoring, optimization and control based on the model proposed in this work is now in progress.

Acknowledgments

This work was financed by the Portuguese Foundation for Science and Technology within the activity of the Research Unit IEETA-Aveiro and the Research Unit ISR-Porto, which is gratefully acknowledged.

Appendix A

Based on the following system of chemical reactions [11]:

$$H_2O \rightleftharpoons H^+ + OH^-,$$

$$H_3PO_4 \rightleftharpoons H^+ + H_2PO_4^-,$$

$$H_2PO_4^- \rightleftharpoons H^+ + HPO_4^{2-},$$

$$HPO_4^{2-} \rightleftharpoons H^+ + PO_4^{3-},$$

$$CaHPO_4 \rightleftharpoons Ca^{2+} + HPO_4^{2-},$$

$$CaPO_4^- \rightleftharpoons Ca^{2+} + PO_4^{3-},$$

$$CaH_2PO_4^+ \rightleftharpoons Ca^{2+} + H_2PO_4^-,$$

$$CaOH^+ \rightleftharpoons Ca^{2+} + OH^-,$$

$$CaHPO_4 \rightleftharpoons Ca^{2+} + HPO_4^{2-}$$

system (A.1) of nonlinear equilibrium equations was built to describe the composition of the solution, as follows:

$$K_1 = y_1^2[H^+][OH^-],$$

$$K_2 = \frac{y_1^2[H^+][H_2PO_4^-]}{[H_3PO_4]},$$

$$K_3 = \frac{y_2[H^+][HPO_4^{2-}]}{[H_2PO_4^-]},$$

$$K_4 = \frac{y_1 y_3 [H^+][PO_4^{3-}]}{y_2 [HPO_4^{2-}]},$$

$$K_5 = \frac{y_2^2 [Ca^{2+}][HPO_4^{2-}]}{[CaHPO_4]},$$

$$K_6 = \frac{y_2 y_3 [Ca^{2+}][PO_4^{3-}]}{y_1 [CaPO_4^-]},$$

$$K_7 = \frac{y_2 [Ca^{2+}][H_2PO_4^-]}{[CaH_2PO_4^+]},$$

$$K_8 = \frac{y_2 [Ca^{2+}][OH^-]}{[CaOH^+]},$$

$$\sigma = \sqrt{\frac{y_2^2 [Ca^{2+}][HPO_4^{2-}]}{K_{ps}}}, \tag{A.1}$$

$$\sigma = \frac{[Ca^{2+}]1000 \times 40.082}{f_1 - f_2},$$

$$f_1 = 9.1083\text{pH}^4 - 246.5800\text{pH}^3 + 2521.1000\text{pH}^2 - 11562\text{pH} + 20138,$$

$$f_2 = \frac{-4.1187\text{pH}^4 + 100.4689\text{pH}^3 - 891.8019\text{pH}^2 + 3373.7539\text{pH} - 4479.3947}{5/(t(^\circ\text{C}) - 25)},$$

$$\text{TCA} = [Ca^{2+}] + [CaHPO_4] + [CaPO_4^-] + [CaH_2PO_4^+] + [CaOH^+],$$

$$\text{TPO} = [H_3PO_4] + [H_2PO_4^-] + [HPO_4^{2-}] + [PO_4^{3-}] + [CaHPO_4] + [CaPO_4^-] + [CaH_2PO_4^+],$$

$$I = \tfrac{1}{2}([OH^-] + [H_2PO_4^-] + 4[HPO_4^{2-}] + 9[PO_4^{3-}] + [H^+] + 4[Ca^{2+}] + [CaPO_4^-] + [CaOH^+] + [CaH_2PO_4^+]),$$

$$y_1 = 10^{(-(0.51\sqrt{I})/(1+\sqrt{I}))},$$

$$y_2 = 10^{(-(4\cdot 0.51\sqrt{I})/(1+\sqrt{I}))},$$

$$y_3 = 10^{(-(9\cdot 0.51\sqrt{I})/(1+\sqrt{I}))},$$

$$\text{pH} = -\log(y_1[H^+]).$$

All chemical species present in the solution and the changes in the speciation of the solution along time were quantified by on-line measurements of the temperature, pH and the calcium concentration, assuming the following values of the equilibrium constants:

$K_1 = 1 \times 10^{-14}$,

$K_2 = 7.11 \times 10^{-3}$,

$K_3 = 6.31 \times 10^{-8}$,

$K_4 = 4.52 \times 10^{-13}$,

$K_5 = 1/264$,

$K_6 = 1/(2.9 \times 10^6)$,

$K_7 = 1/8.48$,

$K_8 = 1/20$,

$K_{ps} = e^{(-(8403.5/T)+41.863-0.09678T)}$ with $T = 273.15 + t(^\circ\text{C})$.

System (A.1) was validated by conductivity measurements. The concentration and the type of precipitate were also determined from (A.1). System (A.1) is the basis for getting Eq. (2) in the macro model discussed in Section 3.1.

References

[1] F. Abbona, H.E. Lundager, Madsen, R. Boistelle, J. Crystal Growth 74 (1986) 581.
[2] J.S. Sorensen, H.E. Lundager Madsen, J. Crystal Growth 216 (2000) 399.
[3] A. Ferreira, C. Oliveira, F. Rocha, J. Crystal Growth 252 (2003) 599.
[4] R.W. Marshall, G.H. Nancollas, J. Phys. Chem. 73 (14) (1969) 3838.
[5] H. Hohl, P.G. Koutsoukos, G.H. Nancollas, J. Crystal Growth 57 (1982) 325.
[6] J.C. Heughebaert, J.F. Rooij, G.H. Nancollas, J. Crystal Growth 77 (1986) 192.
[7] A.D. Randolph, M.A. Larson, Theory of Particulate Processes—Analyses and Techniques of Continuous Crystallisation, Academic Press, New York, 1988.
[8] N.S. Tavare, J. Garside, Chem. Eng. Sci. 48 (3) (1993) 475.
[9] P. Georgieva, S. Feyo de Azevedo, M.J. Goncalves, P. Ho, Chem. Eng. Technol. 3 (3) (2003) 146.
[10] A. Simoglou, P. Georgieva, E.B. Martin, J. Morris, S. Feyo de Azevedo, Comput. Chem. Eng. 29 (6) (2005) 1411.
[11] C. Oliveira, A. Ferreira, F. Rocha, Dicalcium phosphate dihydrate precipitation. Characterization and crystal growth. Annual report of Process System Engineering Research Group, FEUP, Portugal.
[12] P. Ditl, L. Beranek, Z. Rieger, Zuckerind 115 (1990) 667.
[13] P. Georgieva, M.J. Meireles, S. Feyo de Azevedo, Chem. Eng. Sci. 58 (2003) 3699.
[14] H.M. Hulburt, S. Katz, Chem. Eng. Sci. 18 (1964) 555.
[15] R. David, J.M. Bossoutrot, Chem. Eng. Sci. 51 (21) (1996) 4939.
[16] H. Muhr, R. David, J. Villermaux, P.H. Jezequel, Chem Eng. Sci. 51 (2) (1996) 309.
[17] P. Koutsoukos, et al., J. Am. Chem. Soc. 102 (1980) 1553.
[18] O. Sohnel, J.W. Mullin, J. Crystal Growth 60 (1982) 239.
[19] R. David, P. Marchal, J.P. Klein, J. Villermaux, Chem. Eng. Sci. 46 (1991) 1129.